Polym. Bull. (2017) 74:145–165
DOI 10.1007/s00289-016-1704-5

ORIGINAL PAPER

Quiescent and shear-induced non-isothermal crystallization of isotactic polypropylene-based nanocomposites

Clara Silvestre[1] · Marilena Pezzuto[1] · Donatella Duraccio[2] · Geoffrey R. Mitchell[3] · Sossio Cimmino[1]

Received: 25 November 2015 / Revised: 23 February 2016 / Accepted: 19 May 2016 /
Published online: 6 June 2016

Abstract The paper reports a study of the effect of the addition of clay nanoparticles on melt rheology, phase structure, and non-isothermal crystallization process of isotactic polypropylene/hydrogenated oligocyclopentadiene (iPP/HOCP) system in quiescent conditions by DSC and under shear applied at different temperatures by SAXS. For both crystallization conditions, the addition of clay and/or HOCP shifts always the crystallization onset to lower values with respect to iPP. These results can be attributed to the diluent effect of HOCP that causes a decrease in the rate of nucleation and grow of the crystals, to the presence of segregated non-crystallizable phases/particles which hinder the transport of macromolecules chains toward the growing nuclei, and to the formation of beta iPP crystals and in the case of shear-induced crystallization to the presence of HPS which seems to reduce, mainly at low T_s, the amount of oriented polymer crystals, which are nuclei for the crystallization. At a given composition, the crystallization temperatures related at the crystallization under shear are always higher that those obtained by quiescent crystallization supporting the idea that the presence of extended chains in these samples act as nucleating agents favoring the crystallization process of iPP.

✉ Clara Silvestre
clara.silvestre@ipcb.cnr.it

[1] Istituto per i Polimeri, Compositi e Biomateriali, Consiglio Nazionale delle Ricerche (IPCB/CNR), Via Campi Flegrei 34, Pozzuoli, 80078 Naples, Italy

[2] Istituto per le Macchine Agricole e Movimento Terra, Consiglio Nazionale delle Ricerche (IMAMOTER-CNR), Strada delle Cacce 73, 10135 Turin, Italy

[3] Centre for Rapid and Sustainable Product Development, Institute Polytechnic of Leiria, Marinha Grande, Portugal

Introduction

Isotactic polypropylene (iPP) is an important commodity polymer extensively applied in the field of packaging, where its films hold a prominent position because of their transparency, brilliance, low specific weight, chemical inertness, and good processability. Unfortunately, polypropylene, such as other polyolefins, is characterized by low barrier properties, which results in the poor protection of the packaged food [1, 2]. To overcome polypropylene drawbacks, several strategies have been proposed: the most followed ones are to optimize preparation conditions, to add a second component or to use multilayers films, and lately to prepare iPP-based nanocomposites [3–8].

Isotropic films of isotactic polypropylene iPP/hydrogenated oligocyclopentadiene (HOCP) blends were introduced some years ago [9–15]. HOCP is an amorphous, low molecular mass resin with glass transition at about 89 °C. HOCP is constituted by a mixture of *cis* and *trans* isomers, hydrogenated after oligomerization. The iPP/HOCP system was studied by several investigators, and various papers have been published concerning the blends and the commercial isotropic films [9–15]. In particular, Silvestre et al. [11, 13–15] made an extensive study aimed at defining the phase diagram of the system. They detected, for the iPP/HOCP system, the existence of both upper and lower cloud point curves (UCP and LCP curves). Further studies showed that for given conditions of preparation (melting temperature, composition, and rate of cooling), the iPP/HOCP films could present reduced permeability to oxygen and to aroma, together with the increase of elastic modulus and optical properties, compared with that of the pure iPP film. Moreover, it was found that the HOPC, acting as diluent for iPP, caused a decrease of the overall crystallization rate in isothermal conditions.

Recently, with the introduction of nanotechnology and the availability of nanoscale fillers, mainly silicates, it was clear that polymer properties, especially barrier properties, could be improved by adding few percent of nanoparticles. Polymer-layered silicate nanocomposites have attracted great interest, both in industry and in academia, because they often exhibit remarkable improvement in properties when compared with virgin polymer or conventional micro- and macrocomposites [16–18].

These improvements can include higher moduli [16–21], increased strength and heat resistance [22], decreased gas permeability [23–27] and flammability [28], and increased biodegradability rate in the case of matrices made of biodegradable polymers [29]. The properties of the nanocomposites depend not only on the kind of constituents and composition, but mainly on the degree of dispersion of nanoscale particles inside the matrix. When the nanoparticles are well dispersed in the matrix, their large interfacial area and nanoscopic dimension of the particles lead to the formation of hybrid structures which fundamentally differentiates polymer nanocomposites from the traditional filled plastic [30–33].

Therefore, to further increase the properties of iPP/HOCP blend, it was planned to prepare nanocomposites adding to the iPP/HOCP blend few percent of silicate nanoparticles, in particular, a commercial montmorillonite clay.

This paper reports the study of non-isothermal crystallization process of iPP/HOCP-based nanocomposites in quiescent conditions by DSC and under shear applied at different temperatures by SAXS, together with the analysis of the melt rheology.

The non-isothermal crystallization studies have drawn much interest in recent years, because they implies the possibility of controlling and predicting the final morphologies and the properties of semi-crystalline polymers in current transformation processes, such as injection molding or extrusion, where due to flow and non-isothermal conditions, both nucleation and growth are very different from those encountered under quiescent isothermal conditions [34–36].

For crystallizable polymer-blend-based nanocomposites, several processes, such as crystallization, phase separations, and intercalation of polymer molecules into the galleries of clays, must be taken into account to define the phase structure and the final morphology of these systems [37, 38].

Experimental part

Materials

The following materials were used: isotactic polypropylene (iPP), hydrogenated oligocyclopentadiene (HOCP), and clay (Dellite HPS). The isotactic polypropylene (iPP) is a commercial product, trade name Moplen S30S, kindly provided by Basell, Ferrara, Italy. Moplen S30S has melt flow index (MFI) = 1.8 g/10 min and weight molecular mass (Mw) = 2.7 10^5 g/mol.

The hydrogenated oligocyclopentadiene (HOCP) is a hydrogenated mixture of isomers of cyclopentadiene, provided by Exxon Mobile Chemical Europe with trade name Escorez 5340. It has Mw = 680 g/mol and glass transition (T_g) = 89 °C.

The clay used is a naturally occurring purified montmorillonite, kindly supplied by Laviosa Chimica Mineraria SpA, Italy, with trade name Dellite HPS.

Throughout the paper, the following abbreviation will be used for the materials: "iPP" for the isotactic polypropylene Moplen S30S; "HOCP" for the hydrogenated oligocyclopentadiene Escorez 5340; and "HPS" for the clay Dellite HPS.

Sample preparation

The samples for the investigation were prepared by melt mixing in a Brabender-like apparatus at 210 °C and 40 rpm for 10 min.

The amount of the HOCP is kept always at 30 % in weight of the blend. The amount of clay added to the blend was fixed to be 1 g for every 100 g of iPP + HOCP. This amount was chosen after preliminary trials focused on two different amounts of clay (1 and 2 %) added to iPP. The sample with higher amount (iPP/HPS 98/2) presented a very inhomogeneous morphology with large particles aggregates. The compositions of the systems are given in Table 1.

Slabs with a rectangular shape 1 × 70 × 110 mm were prepared by compression molding. A mold containing the polymer material was inserted among the plates of

Table 1 Compositions of the systems prepared by melt mixing

Sample	iPP (%wt)	HOCP (%wt)	HPS pph[a]
iPP	100	–	–
iPP/HPS	99	–	1
iPP/HOCP	70	30	–
iPP/HOCP/HPS	70	30	1

[a] pph = part (or grams) per hundred parts (or grams) of iPP + HOCP

a press at 210 °C without applied force to allow complete melting of the polymer material for 3 min; then, the force was raised to 10,000 lb (pressure on the mold about 833 psi); then, after other 3 min, the plates of the press, fitted with cooling coils, were rapidly cooled to room temperature using cold water. Finally, the force was released, and the mold, removed from the press, was open to take out the slab.

Techniques

Rheological measurements

The rheological measurements were performed in a Thermo Scientific Haake Reostress 6000, using parallel plate–plate geometry. The disk-shaped samples with diameter of 2 cm and a thickness of 1.0 cm were prepared by compression molding in the same conditions of the slabs preparation (see paragraph "Sample preparation"). The steady shear viscosity (η) with respect to shear rates ($\dot{\gamma}$) was recorded. Shear rate $\dot{\gamma}$ is controlled from a remote-programmable controller, and it can be continuously varied to give shear rates between 0.01 and 10 s^{-1}. In the parallel plate instrument, two plates with the diameter of 2.5 cm and the gap size of 0.5 mm were used. All the measurements were performed at different temperatures ($T = 165$, 170, 175, 180, 185, 190 °C).

The temperature dependence of the apparent viscosity was analyzed using the Arrhenius relation

$$\ln\eta_a = \ln A + E_a/RT \tag{1}$$

where A is a material constant, R is the universal gas constant, and E_a is the flow activation energy. From the plots of ln ηa versus $1/T$ at different shear rates, the flow activation energy E_a values can be measured. Equation 1 was used to investigate the temperature dependence of the apparent viscosity.

Structural and morphological analysis

Wide angle X-ray diffraction (WAXD) WAXD analysis was carried out using a Philips diffractometer with Cu Kα radiation (1.542 Å) filtered by nickel. The profiles were recorded with a continuum scan of the Bragg angle 2θ in the angular range 2°–45° with a step scan procedure, at room temperature with a scan rate of 0.02 °C/min and time per step 2.0 s.

Optical microscopy The morphology of the blends was studied using a Zeiss Axioscop polarizing optical microscope, fitted with a Linkam TH600 hot stage. The film inserted between two microscope cover glasses was heated at 200 °C to study the structure of the melt with parallel polars, then the sample was cooled at room temperature at 20 °C/min and the crystalline morphology was analyzed using crossed polars.

Non-isothermal crystallization

Non-isothermal crystallization under quiescent conditions Non-isothermal crystallization under quiescent conditions was investigated by DSC (Mettler DSC822) with the following procedure: the raw sample was heated first to 210 °C and kept for 5 min in the cell to destroy any nuclei that might act as seed crystals. Then, the sample was cooled at a constant rate of 10 °C/min. The exothermic crystallization peak was recorded as a function of temperature during the cooling process.

Non-isothermal crystallization under shear Non-isothermal crystallization under shear was studied using time-resolving in situ small-angle X-ray scattering. SAXS measurements were carried out at the SAXS synchrotron beamline at "European Synchrotron Radiation Facility" (SRF) Grenoble, France, beamline 16 (synchrotron wavelength = 0.4795 Å) and at the NCD beam line at Elettra.

In-situ small-angle x-ray scattering (SAXS) procedures to characterise the structures which develop during shearing and the crystallization which takes place on cooling using a specially designed parallel-plate shear-flow system in conjunction with the intense X-ray beams available at a synchrotron radiation source. The shear stage was placed perpendicular to the incident X-ray beam. Two-dimensional scattering patterns were obtained by means of a MarCCD 165 X-ray detector with resolution 2048 × 2048 pixels.

Essentially, the sample is held between two thin mica disks supported on slotted plates within a small oven equipped with electrical heaters and a refrigerated gas cooling system. This temperature control system provided heating rates up to 20 °C/min and cooling rates up to 10 °C/min. This flow system allows X-ray and neutron scattering experiments to be performed during and following controlled shear flow. The incident X-ray beam lies normal to the plane of the sample and to the flow direction. The sample was placed at a distance of 6 m from the detector.

The slots in the metal plates allowed the X-ray beam to pass through the sample for ~85 % of a revolution. Collimation and masks prior to the rotating plate in the beam line were used to minimise the parasitic scattering from the spokes of the rotating plate, as they cut the incident beam. An intelligent motor control system ensured that when the rotation was stopped, this took place at a rotation angle, where the beam was not obscured by a metal spoke.

The parallel plate system means that the shear rate varies linearly across the radius. The small beam size is <1 mm means that the spread of shears probed by the

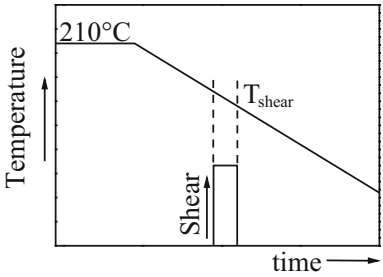

Fig. 1 Schematic of the temperature and shear conditions as a function of time during in situ SAXS experiments

X-ray beam is <5 %. Ex-situ experiments can benefit from the range of shear rates imposed on the sample by selecting different regions to probe.

Pre-molded samples with 1 mm in thickness and 19 mm in diameter were used in these experiments.

All polymer samples were subjected to the following thermal history: the samples were heated to 210 °C and held for 10 min, and then, the melt was cooled at 10 °C/min to room temperature. A step shear of 100 s was applied for each temperature (T_{shear}) of 165, 170, 175, 180, 185, and 190 °C. The shear rate was fixed at 10 s^{-1}. The thermal program used is shown in Fig. 1.

SAXS images were collected continuously, before, during, and after the cessation of the applied shear. The data acquisition time for each scattering pattern (image) was 3 s, with a pause time of 5 s between adjacent images. It should be noted that the scattering images represent the average of the scattered intensity from the scatterers across the thickness of the sample [39].

Each frame of the SAXS data was used to obtain quantitative structural information. The invariant Ω [40] is the total scattering power of the system (Eq. 2), which is independent of the size and the shape of the scattering entities.

$$\Omega = \int_0^\infty I(q)q^2 \mathrm{d}q. \tag{2}$$

The invariant for a two-phase lamellar structure is a function of the volume fraction crystallinity.

Moreover, the total SAXS-integrated intensity from the polymer sample can be separated into two components: one arising from the randomly distributed scatterers in the sample (isotropic contribution) and the other originated by the oriented species (anisotropic contribution) [41, 42].

The total intensity is, therefore, represented as:

$$I_{tot} = I_{iso} + I_{or}. \tag{3}$$

The isotropic component is azimuthally independent (I_{iso}), whereas the anisotropic contribution exhibits dependence on the azimuthal angle (I_{or}). Such an approach implies that I_{iso} arises only from randomly distributed objects, whereas every oriented scatterers in the sample will contribute to the total intensity only with an isotropic intensity.

The fraction of oriented polymer crystals can be obtained as follows:

$$\phi_{\text{or}}^{\text{cryst}} = \frac{I_{\text{or}}(T)}{I_{\text{total}}(T)}. \tag{4}$$

For the samples containing the clay, the fraction of oriented polymer crystals ($\phi_{\text{or}}^{\text{cryst}}$) can be obtained as follows:

$$\phi_{\text{or}}^{\text{cryst}} = \frac{I_{\text{or}}(T) - I_{\text{clay}}(T)}{I_{\text{total}}(T) - I_{\text{clay}}(T)} \tag{5}$$

where T is the temperature at which was applied the shear.

Results and discussion

Rheological analysis

The steady shear viscosity as a function of shear rate for all the systems has been investigated in the range of temperature from 190 to 165 °C.

The analysis indicated that for all the samples, the viscosity drops as the temperature increases and that, at low shear rates, a Newtonian behaviour is followed, with apparent viscosity almost independent of shear rate, whereas at higher shear rates [41], a non-Newtonian flow behaviour with marked shear thinning is observed. See Fig. 2 which reports the rheological behaviour of the systems under investigation at two temperatures, 190 and 170 °C.

For the iPP/HPS system (Fig. 2a), it is interesting to observe that both at 190 and 170 °C; in the Newtonian region, the viscosities are slightly higher with respect to neat iPP, whereas at high shear rates, the viscosities of the composites are generally comparable with that of the iPP matrix indicating that the shear thinning is dominated by that of pure polymer matrix, in agreement with results reported in the literature for other polymer/clay hybrid materials [43].

For the iPP/HOCP system (Fig. 2b), the typical effect of the addition of a plasticizer to a thermoplastic matrix is observed. The presence of a plasticizer decreases the viscosity and elasticity of the neat polymer. However, for obtaining such effects, the amount of plasticizer has to be enough to ensure interconnectivity of the low molecular phase [44, 45].

The curves reported in Fig. 2b demonstrate that the viscosity of the iPP/HOCP blends is lower than that of the iPP, indicating that the 30 % HOCP added to iPP can create gaps between the iPP polymer chains for greater mobility and reduces interchain interactions increasing the interconnectivity of iPP phase and resulting in a rapid percolation of the HOCP.

The rheological behaviour for the ternary systems, iPP/HOCP/HPS (Fig. 2b), is dependent on the shear rate: at low shear rate, the ternary system has similar behaviour of the binary iPP/HOCP system; in the shear thinning region, a decrease of the shear rate steady viscosity is observed with respect to iPP and iPP/HOCP system; the decrease is more evident at higher temperature (190 °C).

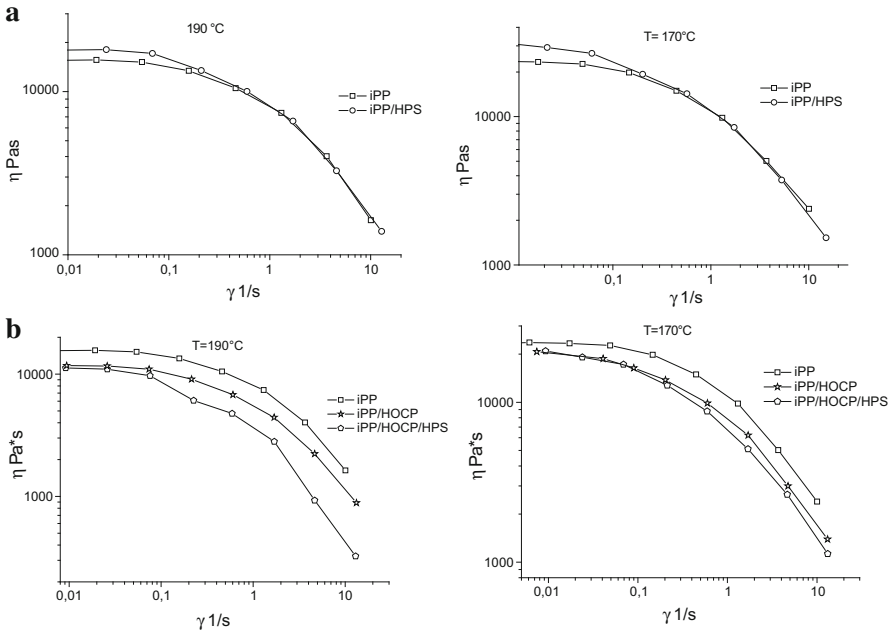

Fig. 2 Rheology behaviour for the systems iPP and iPP/HPS (**a**), and iPP/HOCP and iPP/HOCP/HPS (**b**) at 190 and 170 °C

The Arrhenius plots of ln ηa versus $1/T$ at different shear rates are shown in Fig. 3. From the plots, it can be deduced that the temperature dependence of the apparent viscosity can be well described by the Arrhenius relation. The flow activation energy E_a at a constant shear rate is determined from the slope of the line by performing the least square fit to the plots. The value of E_a reflects the temperature sensitivity of the apparent viscosity. The higher the E_a is, and the stronger temperature sensitivity the apparent viscosity is. The values of E_a at different shear rates are listed in Table 2. For iPP and the binary systems iPP/HPS and iPP/HOCP, the viscous activation energy E_a decreases with the increase of the shear rate. No significant effect of HOCP amount on E_a is found comparing to plain iPP. However, a different effect is showed by the ternary system. The E_a value for the system iPP/HOCP/HPS (Table 2) is always higher than that of iPP and binary systems. This large effect of the HPS on iPP/HOCP blends can lead to the hypothesis that a good swelling of the clay and the oligomer is present. The clay seems to have a better affinity for the oligomer with respect to iPP and should be dispersed more in this phase with respect to iPP. In the low molecular mass phase, the clay could orient easily explaining the decrease in the viscosity and the big increase of flow activation energy for iPP/HOCP/HPS.

Phase structure and morphology

The optical micrographs of the melt at 200 °C of all samples are reported in Fig. 4.

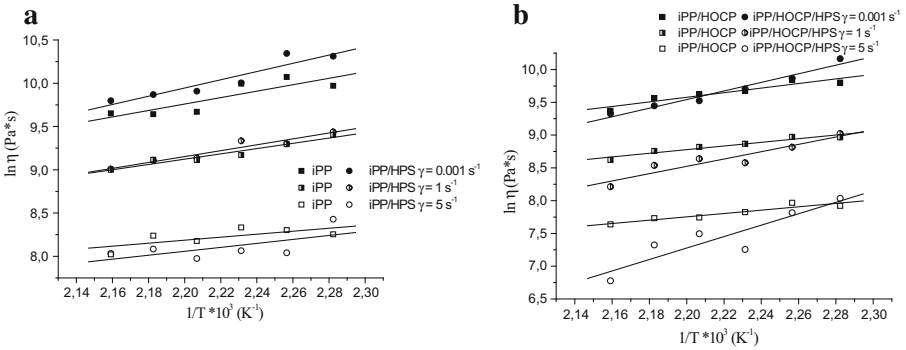

Fig. 3 Arrhenius plot of iPP and iPP/HPS (**a**), and iPP/HOCP and iPP/HOCP/HPS (**b**) at constant shear rate

Table 2 Values of E_a of iPP, iPP/HPS, iPP/HOCP, and iPP/HOCP/HPS at different shear rates

Sample	E_a (kJ/mol) at γ (s^{-1}) = 0.01	E_a (kJ/mol) at γ (s^{-1}) = 1	E_a (kJ/mol) at γ (s^{-1}) = 5
iPP	31	25	14
iPP/HOCP	29	23	21
iPP/HPS	39	28	22
iPP/HOCP/HPS	54	54	72

A homogenous melt is observed for the plain iPP. A phase separated melt is shown by the system iPP/HOCP with spherical domains in a homogeneous matrix. In agreement with the literature results, we can attribute the spherical domains to the HOCP rich phase and the matrix to iPP rich phase [9–11].

The melt morphology of the iPP/HOCP/HPS system is more complex. From the micrograph, it seems that two different kinds of domains are present in the matrix, small spherical domains with narrow size distribution similar to those observed in the binary iPP/HOCP blends and larger domains with broad size distribution. This observation leads to the hypothesis that the system in the melt/amorphous phase could be separated in several phases.

During crystallization, in all samples, a new phase constituted by the iPP crystals develops. Optical micrographs of all samples after non-isothermal crystallization at 10 °C/min are reported in Fig. 5. Spherulites with the average dimension of 20 μm are observed in plain iPP (Fig. 5a). Adding HOCP to iPP, the spherulites of iPP rich phase inglobe the small domains of the HOCP rich phase, whereas the dimension of spherulites increase due to the diluent effect of HOCP on the nucleation process (Fig. 5c).

For the iPP/HPS (Fig. 5b) system, some bright spherulites with negative birefringence are evident that according to the literature, results can be attributed to polypropylene crystallized in beta form [46–48].

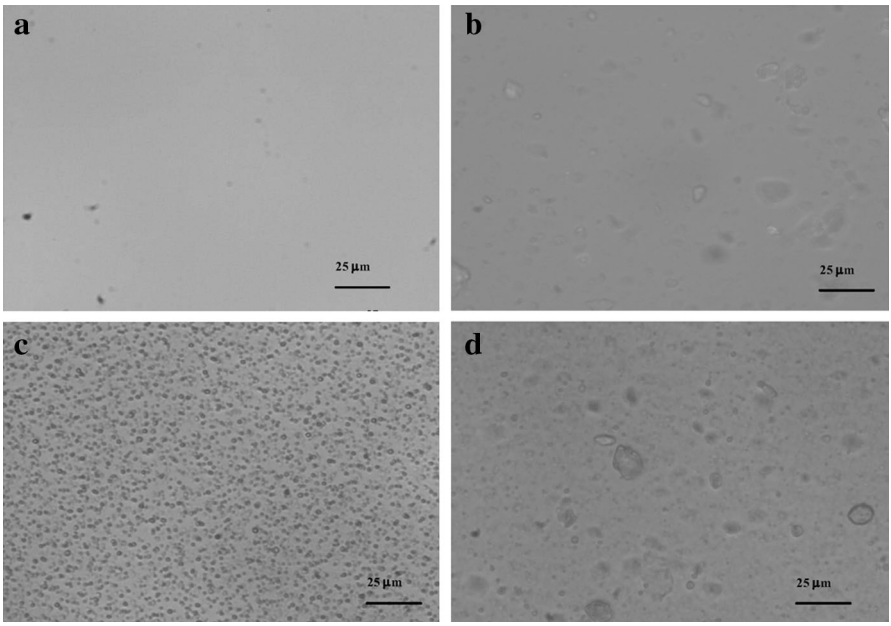

Fig. 4 Optical micrographs of iPP (**a**), iPP/HPS (**b**), iPP/HOCP (**c**), and iPP/HOCP/HPS (**d**) in the melt at 200 °C

WAXS patterns for all the samples, after non-isothermal crystallization, are reported in Fig. 6. For all samples, the presence of the intensity of 111 reflection at 2θ between 18° and 19° indicates that the crystals are mainly organized according to the monoclin α form. Only for iPP/HPS, a small peak at $2\theta \sim 15.9°$ can be observed, characteristics of β form. This result is in agreement with the iPP/HPS optical micrograph reported before (Fig. 5b). The analysis of the diffraction patterns of the system containing clay at low 2θ values (between 2° and 10°) clearly reveals that the reflection corresponding to the interlayer distance of clay platelets ($2\theta = 6.9°$) does not shift with respect to the reflection of neat clay (see Fig. 6). This indicates that no intercalation of the clay layers has been achieved both in the binary and ternary systems.

Non-isothermal crystallization in quiescent conditions

The DSC scans recorded during non-isothermal crystallization at cooling rate 10 °C/min are given in Fig. 7. In Fig. 8, the relative crystallinity as a function of time is reported. In Table 3, the values of the crystallization temperatures (T_c) measured at the maximum of the exothermic peaks are reported.

The non-isothermal crystallization behaviour in quiescent conditions depends on composition: for all the systems, the crystallization process shifts to lower temperatures with respect to plain iPP, indicating that a higher under cooling is needed for these systems to crystallize. The shift is more evident for samples containing HOCP.

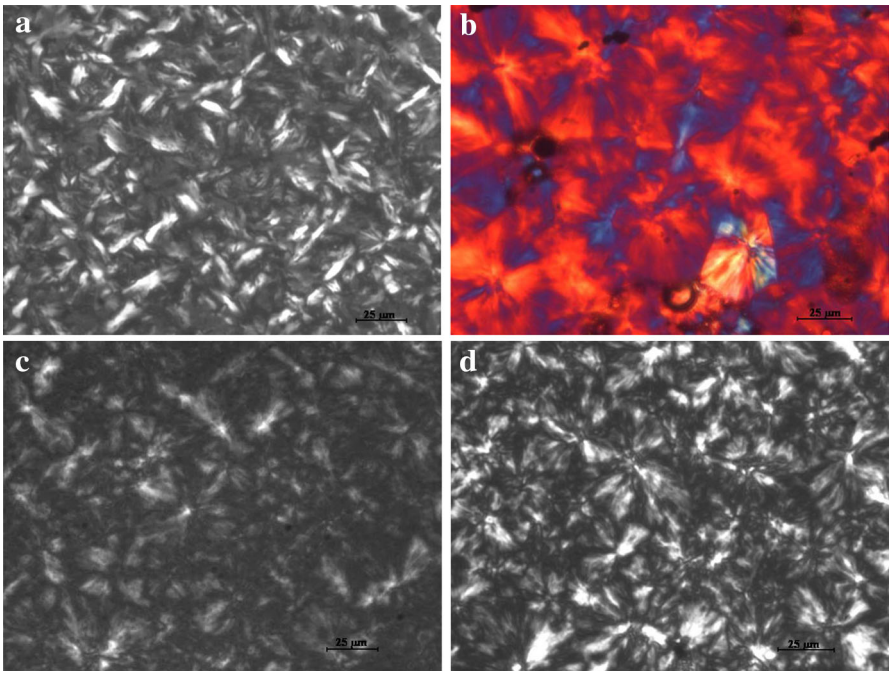

Fig. 5 Optical micrographs of iPP (**a**), iPP/HPS (**b**), iPP/HOCP (**c**), and iPP/HOCP/HPS (**d**) after non-isothermal crystallization at 10 °C/min. The *coloured* micrograph of Fig. 4b was obtained by inserting a quartz plate at 45° between polars (colour figure online)

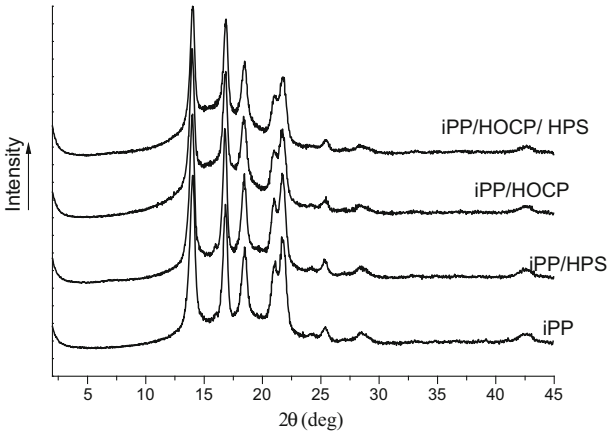

Fig. 6 WAXS patterns for all samples

To explain the crystallization of the systems, it is necessary to take into account the crystallization theory for polymer blends containing one crystallizable component and the phase structure of the systems under investigation. Moreover,

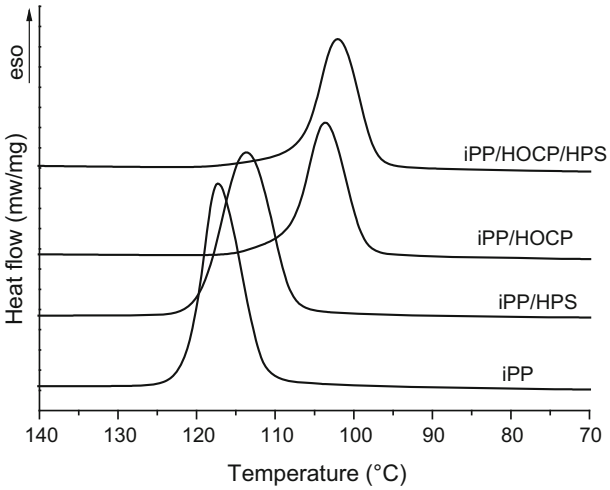

Fig. 7 Non-isothermal crystallization of investigated samples at the cooling rate of 10 °C/min

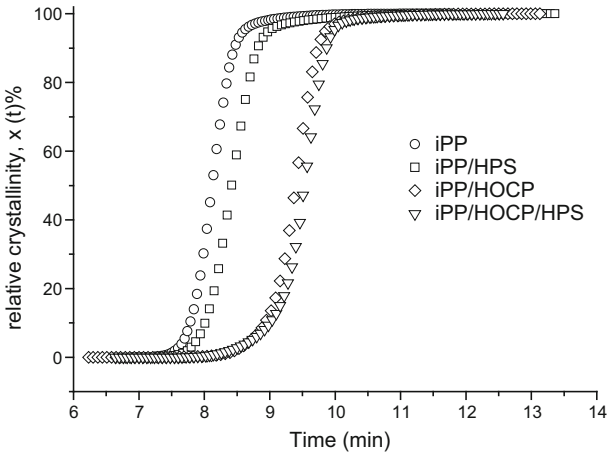

Fig. 8 Relative crystallinity (%) vs time (min)

in the case of a polymorph materials, such as iPP, the formation of different crystals that, as reported in the literature, have different crystallization rates at a given T_c [45–47] needs to be checked.

As reported in the literature, in the temperature range, where the crystallization occurs, the β crystals have a lower spherulite crystallization and nucleation rate. Therefore, for the iPP/HPS system, whose components are immiscible, the shift to lower temperature of the crystallization peak is probably due to the presence of clay particles that hinder the transport of macromolecules chains toward the growing nuclei and to the formation of β crystals: both these phenomena decrease the

Table 3 Crystallization temperature [$T_{c\ (SAXS)}$] at six temperatures at which the shear (T_s) was applied

Sample	$T_{c(SAXS)}$ (°C)						$T_{c\ (DCS)}$ (°C)
	$T_s = 165$ °C	$T_s = 170$ °C	$T_s = 175$ °C	$T_s = 180$ °C	$T_s = 185$ °C	$T_s = 190$ °C	
iPP	153	153	139	133	131	129	117
iPP/HPS	–	152	143	136	130	129	113
iPP/HOCP	151	150	133	124	123	123	103
iPP/HOCP/HPS	135	127	122	119	121	123	102

The last column on the right reports the crystallization temperature, $T_{c(DSC)}$, of the non-isothermal crystallization in quiescent condition

crystallization rate and the value of T_c. For blends containing HOCP, that according to the phase structure analysis is composed of two phases, one rich in the iPP and the other in HOCP, the shift is due to a sum of factors: the diluent effect of HOCP in the iPP rich phase, and the hindering of the transport of macromolecules to the growing spherulites due to the presence of the domains of HOCP rich phase.

For the ternary system, the phase structure is supposed to be probably composed by three phases: a crystallizable iPP rich phase, a non-crystallizable HOCP rich phase, and an HOCP/HPS phase. The diluent effect on both nucleation and sperulite growth rate of HOCP in the iPP rich phase as well as the hinder to the transport of iPP macromolecules chains toward the growing nuclei of the two non-crystallizable phases contribute to the decrease of the crystallization rate (Fig. 8).

Crystallization under shear

Figures 9 and 10 show selected SAXS patterns, vertical flow direction, of iPP at different times after applied shear at 175 and 190 °C, respectively. All the other samples show similar patterns. It is clearly evident that the crystallization behaviour and the resulting morphology depend on the temperature at which the shear has been applied.

At T_s 175 °C (Fig. 9), it can be observed that an orientated superstructure evolved in the polymer melt after the application of the step shear. The equatorial maxima emerged at about 2 min and resulted from the formation of lamellae layers oriented perpendicular to the flow direction. Further cooling produces, the growth of isotropic lamellae that give arise to the scattering ring (image c). As reported in the literature [49–51], the meridional maxima parallel to the flow direction which arise from the formation of "shish" should appear in the very early stage of crystallization. In the patterns reported here, these maxima are hardly detectably. This result could arise from different reasons: (1) low concentration of the shish structures at this share rate; (2) shish structures are too small, so that they are beyond the detection limits of the SAXS setup; (3) as the kebab-like structures grow from the shish, the rod-like scatterer becomes "cylindrical"-like. As this cylinder grows radially, its scattering converges toward the origin and finally disappears [52]. Note that these patterns were obtained at the SAXS beam line which is not

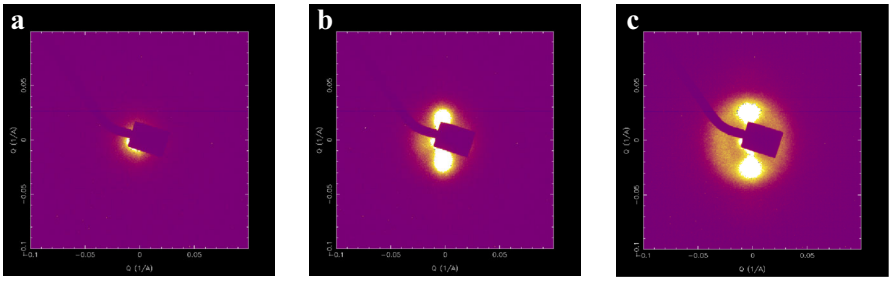

Fig. 9 2D SAXS patterns of iPP melt at selected times after shear at 175 °C

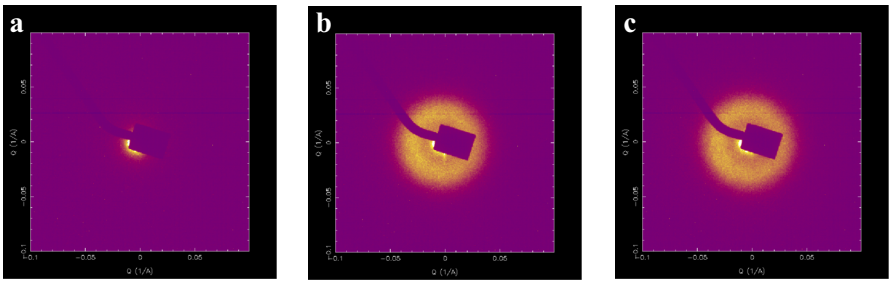

Fig. 10 2D SAXS patterns of iPP melt at selected times after shear at 190 °C

optimized for observing features at very low angles due to the beam collimation and the size and shape of the beam stop which was available.

At higher T_s (Fig. 10), it is clearly evident from the SAXS pattern that the crystallization process is different from the previous one, as shown in Fig. 9; in fact, no oriented structures are detectable, indicating that at the point of crystallization, there was no "memory" of shear deformation.

On the base of the SAXS patterns in dependence of composition and temperatures of the shear during the cooling, the fraction of oriented polymer crystals (ϕ_{or}^{cryst}) and the crystallization temperature T_c can be obtained.

The value of the invariant (calculated by Eq. 2) is proportional to the square of the electron density differences in the sample. In the early stages of crystallization, the value is proportional to the volume fraction of crystals present in the same. The first derivative is a measure of the growth rate of the fraction of crystallinity, and the maximum identifies the temperature at which the sample exhibits the highest growth rate of crystallinity (defined as crystallization temperature T_c) in a similar manner to the peak in the DSC curve during crystallization. Figure 11 shows a plot of the invariant and the derivative, and the similarity to the DSC curve becomes apparent.

As shown by the SAXS patterns in these experiments, in dependence of shear temperatures and composition, some iPP molecules can crystallize on cooling on row nuclei generated by the shear flow that providing a common axis for crystallization, and therefore, these crystals are anisotropically oriented along the axis. Therefore, it becomes interesting to separate out the crystal populations that directed by a row nuclei from that nucleated by random nuclei. To estimate the volume of anisotropic crystals from the SAXS patterns, Eqs. 3, 4, and 5 are used. In Fig. 12, the fraction of oriented polymer crystals ϕ_{or}^{cryst} and the crystallization temperature T_c as a function of shearing temperatures (T_s) are reported.

Figure 12a indicates that for any sample, the fraction of oriented polymer crystals (level of anisotropy) increases by decreasing the temperature at which the shear was applied (T_s), and can be related to the variation in the relaxation processes which take place in the period between the cessation of shear flow and the nucleation of crystallization. In these experiments, a high value of T_s means that as the sample was cooled at a constant rate, the time period between the shear flow and the

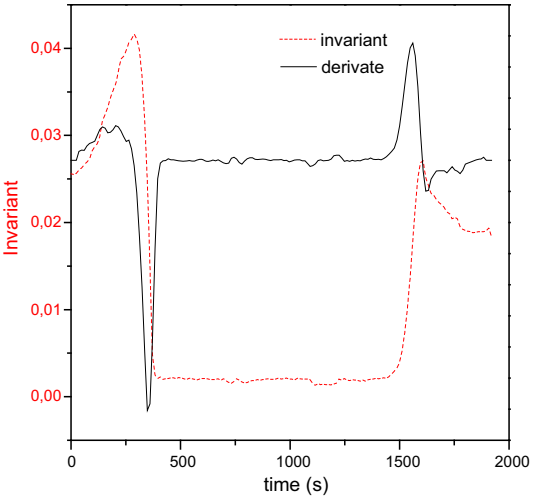

Fig. 11 Example of invariant curve and its derivate

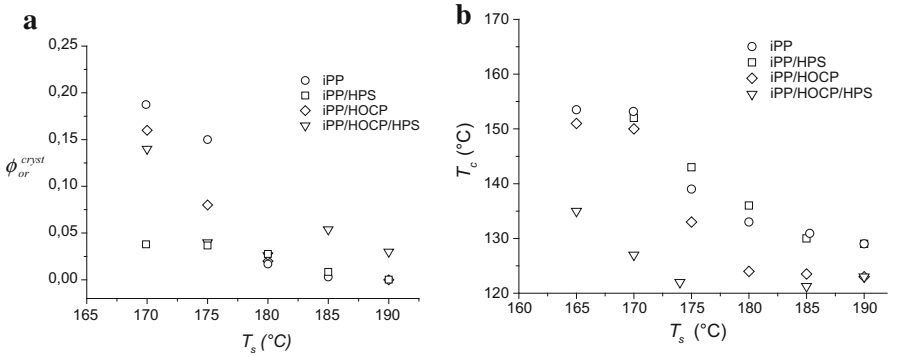

Fig. 12 Orientation (ϕ_{or}^{cryst}) and crystallization temperature (T_c) vs T_s for iPP and iPP/HPS; and iPP/HOCP and iPP/HOCP/HPS

subsequent crystallization is probably longer as a consequence of the greater temperature difference. For a given sample, the higher value of ϕ_{or}^{cryst} at low T_s with respect to the value ϕ_{or}^{cryst} at high T_s is due to the reduction of the 'relaxation' period prior to crystallization that can be insufficient to allow the conformation of the macromolecules to relax to their equilibrium state prior to crystallization.

For of iPP/HPS and iPP/HOCP blend, ϕ_{or}^{cryst} depends on the T_s. At high shear temperatures the level of preferred orientation is similar to that of plain iPP, whereas at low shear temperatures (170 and 175 °C), the following behaviour: ϕ_{or}^{cryst} of iPP/HPS < iPP/HPS < iPP is observed.

The ternary system iPP/HOCP/HOCP presents the peculiar behaviour of ϕ_{or}^{cryst} vs temperature compared with the others compositions. At $T_s < 180$ °C, the orientation of the ternary system is lower than that of iPP; whereas at $T_s > 180$ °C, the orientation is higher.

To verify if there is the clay directs, the crystallization of iPP playing the part of the extended chains (as the shish) during the formation of the oriented superstructures; a Couette style cell is used in the same basic shear cell that replaces the parallel plates (as describe in the experimental chapter). In such an arrangement, the scattering vector lies in the plane containing the flow direction and the velocity gradient.

Figure 13 illustrates selected typical SAXS spectra collected at room temperature (a), in the melt (b), during the shear at 170 °C (c), at the end of the measure at room temperature in the normal (d_1) and in the edge direction (d_2). These patterns clearly show the evolution of oriented structures.

Figure 13 shows a well-developed isotropic ring typical of the semicrystalline polymers prepared by compression molding. No equatorial streaks are present suggesting that the clay layers are not oriented along the flow direction confirming that the HPS is not well dispersed in the polymer matrix. The shearing meridional maxima (due to layer-like oriented structure, or kebab, perpendicular to flow direction) emerge and can be seen at the end of the experiment at room temperature in Fig. 13 d_1 and d_2. Again, in this figure, no clay orientation is present. Moreover, as already stated before, no meridional reflection is detected in the melt. It is possible to conclude that HPS does not act as template for the process of polymer crystallization. iPP melt only retains a memory of the applied shear deformation, which manifest itself through the formation of anisotropic morphology.

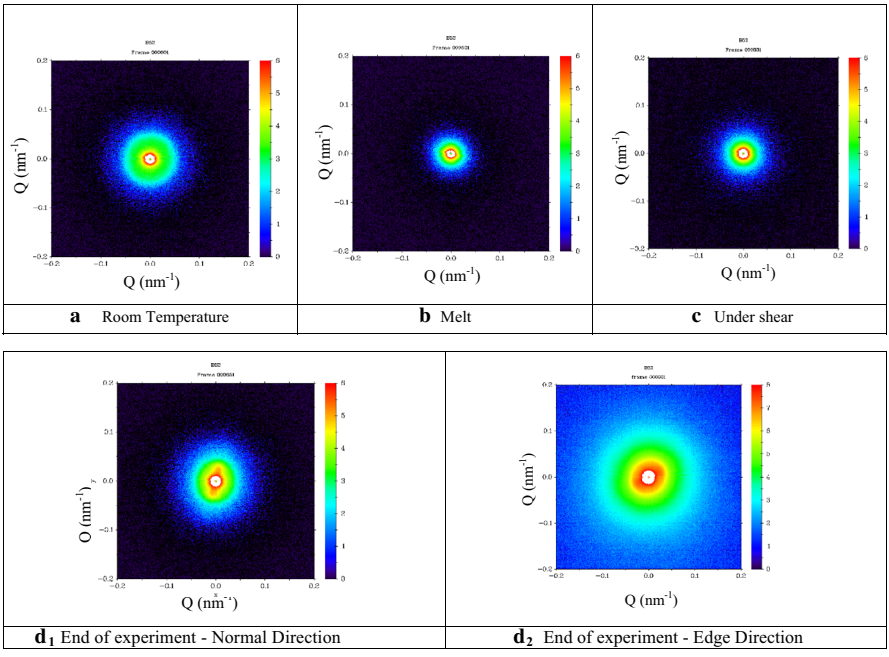

Fig. 13 SAXS patterns for iPP/HPS collected at room temperature (**a**), in the melt (**b**), during the shear at 170 °C (**c**) and at the end of the experiment (room temperature) in the normal (**d_1**) and in the edge direction (**d_2**)

In addition, Fig. 13 d_1 and d_2 shows the classical scattering pattern attributed to iPP shish-kebab lamellar structures.

Figure 12b and Table 3 show T_c vs T_s (temperature at which was applied the shear) for all the samples. It is clear that for all the samples, T_c decreases by increasing T_s in agreement with the DSC non-isothermal data; this behaviour indicates that the crystallization under shear, for all systems to crystallize in comparison with pure iPP, requires a higher undercooling. In this case, the shift to lower temperature is more evident at low T_S and for the ternary system. These results lead to the hypothesis that whereas in quiescent condition, the presence of a partially miscible diluent (HOCP) to iPP is the key factor determining the decrease of the non-isothermal crystallization process; in the case of shear-induced crystallization, an important role is also assumed by HPS that reduces, mainly at low T_s, the presence of oriented polymer crystals that act as nucleating agents.

Conclusions

From the results presented in the paper, the following conclusions can be drawn:

1. The presence of HPS does not modify the rheological behaviour of neat iPP. For the iPP/HOPC blend, a high interconnectivity of this phase is present resulting in a rapid percolation of the HOCP and confirming partial miscibility between the two components. In the ternary system, an interesting effect of HPS on the E_a is found. This could be explained with a good swelling of the clay and the oligomer with HPS that has better affinity for the oligomer with respect to iPP.
2. The non-isothermal crystallization behaviour in quiescent conditions depends on composition The addition of clay and/or HOCP shifts the crystallization onset to lower values indicating that the nucleation process occurs at lower temperature. These results can be attributed to the diluent effect of HOCP (for the binary and ternary blends containing HOCP) and to the presence of segregated non-crystallizable phases/particles that affect the transport of macromolecules chains toward the growing nuclei. To define the crystallization behaviour for iPP/HPS nanocomposites, the influence of iPP β crystals on the crystallization rate must be taken into consideration.
3. The in situ SAXS experiments revealed that the temperature, at which crystal growth rate is at maximum, is strongly dependent on the temperature at which the shear flow was applied. In the melt after shear flow, the polymer chains which were extended will be relaxing towards isotropic state. If crystallization takes place before, the chains are full relaxed, and the extended chains act as row nuclei that has two consequences. The first is a high level of common orientation of the crystals and the second is that the crystallization occurs at higher temperatures. As the polymer crystallizes in any event, the questions are really how much is directed by row nuclei and how much by randomly arrange nuclei. This changes the crystallization temperature and the level of anisotropy. The clay platelet does not template the crystallization. The comparison of the crystallization data leads to the hypothesis that whereas in quiescent condition,

the presence of a partially miscible diluent (HOCP) to iPP is the key factor determining the decrease of the non-isothermal crystallization process; in the case of shear-induced crystallization, an important role is also assumed by HPS that reduces, mainly at low T_s, the presence of oriented polymer crystals.

At the end of this study, it is possible to conclude that the system iPP/HOCP/HPS needs further investigation focused on optimizing the preparation conditions. In fact, in these three component systems, HPS seems to have a better affinity with the HOCP with respect to iPP. Therefore, the modalities of blending could become very important: for example, nanocomposites obtained in two stages with a preliminary preparation of a masterbatch made of HOCP and HPS to add to iPP could bring interesting morphology. The aim of this strategy is to master the competition among different processes (crystallization, phase separation and intercalation of iPP and HOCP into the galleries of HPS clays, and intercalation of HOCP chain and HPS platelets inside the iPP crystalline lamellae) and finally to design new nanomaterials with improved properties. For the ternary system, all these processes (crystallization, phase separation, and intercalations) must be taken into account to define the phase structure and the final morphology and if these process in dependence on crystallization conditions will compete each other. Preliminary results that will be published in a forthcoming paper seem to confirm this hypothesis.

Acknowledgments The research described herein was partially supported by COST Action FA0904 'Eco-sustainable food packaging based on polymer nanomaterials'. The research leading to these results has received funding from the European Community's Seventh Framework Programme (FP7/2007-2013) under Grant Agreement No 226716". The authors are grateful to Dr Ingrid Bernstorff (Electra) and Dr Francois Faust (ESRF) for their involvement in the experiments. The authors are grateful to Profs. Claudio De Rosa and Finizia Auriemma (University of Naples, Federico II) for helpful discussions.

References

1. Vasile C (ed) (2000) Handbook of polyolefins. Marcel Dekker, Inc., New York
2. Kaminsky W (2013) Polyolefins: 50 years after Ziegler and Natta II. Springer, Berlin Heidelberg
3. Vikas M (ed) (2010) Advances in polyolefin nanocomposites. CRC Press, Boca Raton
4. Duraccio D, Silvestre C, Pezzuto M, Cimmino S, Marra A (2013) Polypropylene and polyethylene-based nanocomposites for food packaging applications. In: Silvestre C, Cimmino S (eds) Ecosustainable polymer nanomaterials for food packaging: innovative solutions, characterization needs, safety and environmental issues. CRC Press, Boca Raton, pp 143–67
5. Kurek M, Klepac D, Ščetar M, Galić K, Valić S, Liu Y, Yang W (2011) Gas barrier and morphology characteristics of linear low-density polyethylene and two different polypropylene films. Polym Bull 67:1293–1309
6. Cimmino S, Silvestre C, Duraccio D, Pezzuto M (2013) Effect of hydrocarbon resin on the morphology and mechanical properties of isotactic polypropylene/clay composites. J Appl Polym Sci 119:1135–1143
7. Zehetmeyer G, Soares RMD, Brandelli A, Mauler RS, Oliveira RVB (2012) Evaluation of polypropylene/montmorillonite nanocomposites as food packaging material. Polym Bull 68:2199–2217
8. Ayhan Z, Cimmino S, Esturk O, Duraccio D, Pezzuto M, Silvestre C (2015) Development of films of novel polypropylene based nanomaterials for food packaging application. Packag Technol Sci 28:589–602

9. Cimmino S, Guarrata P, Martuscelli E, Silvestre C, Buzio PP (1991) Morphology, phase structure and thermal behaviour of films of isotactic polypropylene/hydrogenated oligocyclopentadiene blends: 1. Extruded isotropic films. Polymer 32:3299–3304
10. Cimmino S, Guarrata P, Martuscelli E, Silvestre C (1993) Isotactic polypropylene/hydrogenated oligo(cyclopentadiene) blends: phase diagram and dynamic-mechanical behaviour of extruded isotropic films. Polymer 34:972
11. Cimmino S, Di Pace E, Karasz FE, Martuscelli E, Silvestre C (1993) Isotactic polypropylene/hydrogenated oligo(cyclopentadiene) blends: phase diagram and dynamic-mechanical behaviour of extruded isotropic films. Polymer 34:972
12. Cimmino S, Della Vecchia G, Silvestre C (2004) Morphology and properties of isotactic polypropylene modified with hydrogenated hydrocarbon resin: I binary blends. J Appl Polym Sci 92:3454–3465
13. Silvestre C, Cimmino S, Lin JS (2004) Structure, morphology and crystallization process of isotactic polypropylene/hydrogenated hydrocarbon resin blends. J Polym Sci Part B Polym Phys 42:3368–3379
14. Caponetti E, Chillura Martino D, Cimmino S, Floriano MA, Martuscelli E, Silvestre C, Triolo R (1996) Small angle scattering study of the structure of isotactic polypropylene/hydrogenated oligo(cyclopentadiene) blends. J Mol Struct 383:75–79
15. Triolo A, Silvestre C, Cimmino S, Martuscelli E, Caponetti E, Triolo R (1998) Structure of isotactic polypropylene/hydrogenated oligo(cyclopentadiene) blends: I. Polypropylene rich blends. Polymer 39:1697–1702
16. Kamal MR, Uribe-Calderon J (2012) Polymer–clay nanocomposites. Wiley encyclopedia of composites. Wiley, London, pp 1–30
17. Giannelis EP, Krishnamoorti R, Manias E (1999) Polymer-silicate nanocomposites: model systems for confined polymers and polymer brushes. Adv Polym Sci 138:107
18. Gurses A (2015) Introduction to polymer–clay nanocomposites. CRC Press, Boca Raton
19. Vaia RA, Price G, Ruth PN, Nguyen HT, Lichtenhan J (1999) Polymer-layered silicate nanocomposites: an overview. J Appl Clay Sci 15:67
20. Biswas M, Sinha Ray S (2001) Recent progress in synthesis and evaluation of polymer-montmorillonite nanocomposites. Adv Polym Sci 155:167
21. Giannelis EP (1998) Polymer-layered silicate nanocomposites: synthesis, properties and applications. Appl Organomet Chem 12:675
22. Xu R, Manias E, Snyder AJ, Runt J (2001) Low permeability polyurethane nanocomposites. Macromolecules 34:337
23. Bharadwaj RK (1989) Modeling the barrier properties of polymer layered silicate nanocomposites. Macromolecules 2001:34
24. Messersmith PB, Giannelis EP (1047) Synthesis and barrier properties of poly(ε-caprolactone)-layered silicate nanocomposites. J Polym Sci Part A Polym Chem 1995:33
25. Yano K, Usuki A, Okada A, Kurauchi T, Kamigaito O (1993) Synthesis and properties of polyimide–clay hybrid. J Polym Sci Part A Polym Chem 31:2493
26. Kojima Y, Usuki A, Kawasumi M, Fukushima Y, Okada A, Kurauchi T, Kamigaito O (1993) Mechanical properties of nylon 6-clay hybrid. J Mater Res 8:1179
27. Gilman JW, Jackson CL, Morgan AB, Harris R Jr, Manias E, Giannelis EP, Wuthenow M, Hilton D, Phillips SH (2000) Flammability properties of polymer–layered-silicate nanocomposites. Polypropylene and polystyrene nanocomposites. Chem Mater 12:1866
28. Sinha Ray S, Yamada K, Okamoto M, Ueda K (2002) Poly-lactide layered silicate nanocomposites: a novel biodegradable material. Nano Lett 2:1093
29. Novak BM (1993) Hybrid nanocomposite materials—between inorganic glasses and organic polymers. Adv Mater 5:422
30. Messersmith PB, Giannelis EP (1994) Synthesis and characterization of layered silicate-epoxy nanocomposites, chemistry of materials. Chem Mater 6:1719
31. Silvestre C, Cimmino S (eds) (2013) Ecosustainable polymer nanomaterials for food packaging: innovative solutions, characterization needs, safety and environmental issues. CRC Press
32. Cimmino S, Duraccio D, Silvestre C, Pezzuto M (2009) Isotactic polypropylene modified with clay and hydrocarbon resin: compatibility, structure and morphology in dependence on crystallization conditions. Appl Surf Sci 256S:S40–S45

33. Cimmino S, Silvestre C, Duraccio D, Pezzuto M (2011) Effect of hydrocarbon resin on the morphology and mechanical properties of iPP/clay composites. J Appl Polym Sci 119:1135–1143
34. Di Lorenzo ML, Cimmino S, Silvestre C (2001) Non-isothermal crystallization of isotactic polypropylene blended with poly(a-pinene): 1. Bulk crystallization. J Appl Polym Sci 82:358–367
35. Silvestre C, Di Lorenzo ML (1999) Non-isothermal crystallization of polymers. Prog Polym Sci 24:917–950
36. Gao J, Cao X, Zhang C, Hu W (2013) Non-isothermal crystallization kinetics of polypropylene/MAP-POSS nanocomposites. Polym Bull 70:1977–1990
37. De Rosa C, Auriemma F, Di Girolamo R, Aprea R, Thierry A (2011) Selective gold deposition on a nanostructured block copolymer film crystallized by epitaxy. Nano Res 4:241–248
38. Silvestre C, Cimmino S (2003) Crystallization, morphology and melting in polymer blends. In: Vasile C, Kulshreshtha AK (eds) Handbook of blends and composites. Rapra Technology, Shawbury, pp 421–472
39. Nogales A, Thornley SA, Mitchell GR (2004) Shear cell for in situ WAXS, SAXS and SANS experiments on polymer melts under flow fields. J Macromol Sci Physs B43:1161–1170
40. Bowron DT, Soper AK, Jones K, Ansel S, Birch S, Norris J et al (2010) NIMROD: the near and intermediate range order diffractometer of the ISIS second target station. Rev Sci Instrum 81:033905
41. Mitchell GR, Lovell R (1981) Application of cylindrical distribution functions to wide-angle X-ray scattering from oriented polymers. Acta Crystallogr A A37:189
42. Wang Y, Chen FB, Wu KC, Wang JC (2006) Shear rheology and melt compounding of compatibilized-polypropylene nanocomposites: effect of compatibilizer molecular weight. Polym Eng Sci 46:289
43. Krishnamoorti R, Vaia RA, Giannelis EP (1996) Structure and dynamics of polymer-layered silicate nanocomposites. Chem Mater 8:1728
44. Shahbikian S et al (2011) Morphology and rheology of nonreactive and reactive EPDM/PP blends in transient shear flow: plasticized versus nonplasticized blends. Rubber Chem Technol 84:325
45. Shahbikian S et al (2011) Rheology/morphology relationship of plasticized and nonplasticized thermoplastic elastomers based on ethylene-propylene-diene-terpolymer and polypropylene. Polym Eng Sci 11:2314
46. Silvestre C, Cimmino S, Di Pace E (2000) Morphology of polyolefins. In: Vasile C (ed) Handbook of polyolefins: second edition, revised and expanded. Marcell Dekker, New York, pp 175–206
47. Silvestre C, Di Lorenzo ML, Di Pace E (2000) Crystallization of polyolefins. In: Vasile C (ed) Handbook of polyolefins: second edition, revised and expanded. Marcell Dekker, New York, pp 223–242
48. Silvestre C, Cimmino S, Triolo R (2003) Structure, morphology, and crystallization of a random ethylene–propylene copolymer. J Polym Sci Part B Polym Phys 41:493–500
49. Somani RH, Hsiao BS, Agarwal P, Fruitwala H, Tsou AH (2002) Shear-induced precursor structures in isotactic polypropylene melt by in-situ rheo-SAXS and rheo-WAXD studies. Macromolecules 35:9096
50. Schultz JM, Hsiao BS, Samon JM (2000) Structural development during the early stages of polymer melt spinning by in situ synchrotron X-ray techniques. Polymer 41:8887
51. Somani RH, Hsiao BS, Nogales A, Srinivas S, Tsou AH, Sics I, Balta-Calleja FJ, Ezquerra TA (2000) Structure development during shear flow-induced crystallization of i-PP: in-situ small-angle X-ray scattering study. Macromolecules 33:9385
52. Nogales A, Hsiao BS, Somani RH, Srinivas S, Tsou AH, Balta-Calleja FJ, Ezquerra TA (2001) Shear-induced crystallization of isotactic polypropylene with different molecular weight distributions: in situ small- and wide-angle X-ray scattering studies. Polymer 42:5247